THE JOURNAL OF BIOLOGICAL CHEMISTRY VOL. 286, NO. 6, pp. 4049–4058, February 11, 2011

Structural Determinants of an Insect β-*N*-Acetyl-D-hexosaminidase Specialized as a Chitinolytic Enzyme*[S]

Received for publication, September 14, 2010, and in revised form, November 14, 2010 Published, JBC Papers in Press, November 24, 2010, DOI 10.1074/jbc.M110.184796

Tian Liu[‡1], **Haitao Zhang**[§1], **Fengyi Liu**[‡], **Qingyue Wu**[‡], **Xu Shen**[§¶2], **and Qing Yang**[‡‖3]

From the [‡]*Department of Bioscience and Biotechnology, Dalian University of Technology, Dalian 116024, China, the* [‖]*Shanghai Key Laboratory of Chemical Biology, East China University of Science and Technology, Shanghai 200237, China, the* [§]*State Key Laboratory of Drug Research, Shanghai Institute of Materia Medica, Chinese Academy of Sciences, Shanghai 201203, China, and the* [¶]*E-Institutes of Shanghai Municipal Education Commission, School of Medicine, Shanghai Jiaotong University, Shanghai 200025, China*

β-*N*-Acetyl-D-hexosaminidase has been postulated to have a specialized function. However, the structural basis of this specialization is not yet established. OfHex1, the enzyme from the Asian corn borer *Ostrinia furnacalis* (one of the most destructive pests) has previously been reported to function merely in chitin degradation. Here the vital role of OfHex1 during the pupation of *O. furnacalis* was revealed by RNA interference, and the crystal structures of OfHex1 and OfHex1 complexed with TMG-chitotriomycin were determined at 2.1 Å. The mechanism of selective inhibition by TMG-chitotriomycin was related to the existence of the +1 subsite at the active pocket of OfHex1 and a key residue, Trp^{490}, at this site. Mutation of Trp^{490} to Ala led to a 2,277-fold decrease in sensitivity toward TMG-chitotriomycin as well as an 18-fold decrease in binding affinity for the substrate $(GlcNAc)_2$. Although the overall topology of the catalytic domain of OfHex1 shows a high similarity with the human and bacterial enzymes, OfHex1 is distinguished from these enzymes by large conformational changes linked to an "open-close" mechanism at the entrance of the active site, which is characterized by the "lid" residue, Trp^{448}. Mutation of Trp^{448} to Ala or Phe resulted in a more than 1,000-fold loss in enzyme activity, due mainly to the effect on k_{cat}. The current work has increased our understanding of the structure-function relationship of OfHex1, shedding light on the structural basis that accounts for the specialized function of β-*N*-acetyl-D-hexosaminidase as well as making the development of species-specific pesticides a likely reality.

β-*N*-Acetyl-D-hexosaminidase (EC 3.2.1.52), a member of the family 20 glycosyl hydrolyases (GH20),[4] is an enzyme that participates in the breakdown of glycosidic bonds of glycans, glycoproteins, and glycolipids (1). It has been postulated to have specialized physiological functions, including post-translational modification of *N*-glycans, degradation of glycoconjugates, and egg-sperm recognition (1). The structural basis for these specialized functions is still unclear.

It is interesting to note that insects have evolved to have more than one β-*N*-acetyl-D-hexosaminidase, as revealed by genomic analysis of various insects, including Coleoptera, Diptera, Hymenoptera, Lepidoptera, Phthiraptera, and Hemiptera. The activities of insect β-*N*-acetyl-D-hexosaminidases are not restricted to chitin degradation but are also associated with post-translational modification of *N*-glycans, degradation of glycoconjugates, and egg-sperm recognition, suggesting that these enzymes have rather versatile physiological functions in the growth and development of insects (2). Some of these physiological functions may overlap with those of the same enzymes found in higher organisms. Mammal lysosomal β-*N*-acetyl-D-hexosaminidases are mainly responsible for glycoconjugate degradation in lysosome (3). Likewise, β-*N*-acetyl-D-hexosaminidases from the insects *Bombyx mori* (4) and *Spodoptera frugiperda* (5) have broad substrate specificity ranging from *N*-glycans to chitooligosaccharides, suggesting that they have the same function as their mammal counterparts. Mammal β-*N*-acetyl-D-hexosaminidases have been shown to be important for egg-sperm recognition (6), and the enzymes from *Drosophila melanogaster* sperm membrane also participate in the same process (7, 8). Plant β-*N*-acetyl-D-hexosaminidases carry out post-translational modification of *N*-glycans (9, 10). Similarly, the enzymes from *D. melanogaster* (11) and *S. frugiperda* (12) (termed Fdls) also carry out post-translational modification of *N*-glycans, but they have a rather narrow substrate specificity. Comparative analysis of β-*N*-acetyl-D-hexosaminidase genes in the co-

* This work is supported by National Key Project for Basic Research Grants 2010CB126100, 2009CB918502, and 2010CB912501; the Program for New Century Excellent Talents in University; the National Special Fund for State Key Laboratory of Bioreactor Engineering (East China University of Science and Technology, Shanghai, China); National Natural Science Foundation of China Grant 10979072; Key New Drug Creation and Manufacturing Program Grant 2009ZX09301-001; and E-Institutes of Shanghai Municipal Education Commission Grant E09013.

[S] The on-line version of this article (available at http://www.jbc.org) contains supplemental Figs. S1 and S2.

The atomic coordinates and structure factors (codes 3NSM and 3NSN) have been deposited in the Protein Data Bank, Research Collaboratory for Structural Bioinformatics, Rutgers University, New Brunswick, NJ (http://www.rcsb.org/).

[1] These authors contributed equally to this work.

[2] To whom correspondence may be addressed: 555 Zuchongzhi Rd., Shanghai 201203, China. Tel.: 86-21-50806600; Fax: 86-21-50807188; E-mail: xshen@mail.shcnc.ac.cn.

[3] To whom correspondence may be addressed: 2 Linggong Rd. Dalian 116024, China. Tel.: 86-411-84707245; Fax: 86-411-84707245; E-mail: qingyang@dlut.edu.cn.

[4] The abbreviations used are: GH20, family 20 glycosyl hydrolyase(s); ds*OfHEX1*, dsRNA of *OfHEX1*; ds*GFP*, dsRNA for the gene encoding green fluorescent protein; 4MU, 4-methylumbelliferone; triMe, trimethyl.

leopteran, *Tribolium castaneum*, has provided molecular and biological evidence to support the hypothesis that each of the four TcNAGs among a total of seven β-*N*-acetyl-D-hexosaminidases has an essential and specific function in chitin degradation and/or *N*-glycan modification during development (13). Thus, it is interesting to know how these enzymes could carry out their specialized functions in terms of their structural features.

Seven crystal structures of GH20 β-*N*-acetyl-D-hexosaminidases have been obtained, including two human and five bacterial enzymes. Both the human HexA and HexB are the mammal β-*N*-acetyl-D-hexosaminidases that degrade glycoconjugate in the lysosome (14–16). The bacterial enzymes include SpHex (17, 18) and SmCHB (19, 20), which are found in the chitinolytic bacteria *Streptomyces plicatus* and *Serratia marcescens*, respectively; AaDspB, which is from *Aggregatibacter actinomycetemcomitans* and is involved in the degradation of biofilm (polymeric β-1,6-linked GlcNAc) (21); and the enzyme from *Paenibacillus* sp. TS12, PsHex, that can efficiently degrade various glycosphingolipids (22). In addition, PgGcnA, the enzyme found in the endocarditis pathogen, *Streptococcus gordonii*, is involved in the release of dietary carbohydrates (23). To our knowledge, no crystal structure of insect β-*N*-acetyl-D-hexosaminidase has yet been reported.

We have previously identified a β-*N*-acetyl-D-hexosaminidase (OfHex1) from the lepidopteran insect *Ostrinia furnacalis* (Asian corn borer), which we think may be involved in chitin degradation during insect metamorphosis (2). In the present study, we used RNA interference to demonstrate the vital role of OfHex1 during the pupation of *O. furnacalis*. We also resolved the crystal structures of free OfHex1 and OfHex1 in complex with the recently isolated inhibitor TMG-chitotriomycin to 2.1 Å. Structural alignment of OfHex1 with reported β-*N*-acetyl-D-hexosaminidases from humans (14–16) and bacteria (17–23) revealed several unique structural features in OfHex1, which provided further insight into the structural basis of the enzyme's specialized function. Because *O. furnacalis* is a destructive and persistent pest in the Asian and pan-Pacific regions, a greater understanding of the structure-function relationship of OfHex1 would enable the development of a more species-specific pesticide.

EXPERIMENTAL PROCEDURES

Gene Expression and RNAi—O. furnacalis was reared on an artificial diet. To analyze the temporal transcriptional pattern of *OfHEX1* (encoding OfHex1, DQ887769), total RNAs were extracted from the entire insect at the fourth instar larval, fifth instar larval, prepupal, pupal, and adult stages using RNAiso reagent (TaKaRa, Dalian, China). To analyze the transcriptional levels of *OfHEX1* in different tissues, total RNAs were extracted from the integument and alimentary tract of the larva and subjected to RT-PCR using the PrimeScript RT-PCR kit (TaKaRa). The resulting cDNA obtained was subjected to real-time PCR using the *OfHEX1*-specific primers, 5′-TATGGGCATCCAGGCAGAG-3′ (forward) and 5′-AGGAGAGCCCCGTTGTTGT-3′ (reverse), and the *OfRpS3* (encoding ribosomal protein S3, EU275206, as an internal reference)-specific primers, 5′-AGCGTTTCAACATCCCTGAAC-3′ (forward) and 5′-CACACCATAGCAGGCACGA-3′ (reverse). Real-time PCR was performed using the SYBR PrimeScript RT-PCR Kit (TaKaRa) and Rotor-Gene 3000 (Corbett Research, Sydney, Australia).

For double-stranded RNA synthesis, a 246-bp fragment between nucleotides 151 and 356 in *OfHEX1* was selected as template. Two primers, 5′-TAATACGACTCACTATAGGGG-CGTCAAGCTGAAGAAGAACG-3′ (forward) and 5′-TAATACGACTCACTATAGGGAGCGGCCTCCATCAGGT-3′ (reverse), each with a T7 RNA promoter sequence (underlined bases) flanking the 5′-end were used in the *in vitro* transcription performed with MEGAscript RNAi Kit (Ambion, Austin, TX) according to the manufacturer's instructions. Approximately 3 μg of *OfHEX1* dsRNA (ds*OfHEX1*) was injected into the penultimate abdominal segment of day 2–5 instar larvae using a 10-μl syringe. Larvae injected with 3 μg of dsRNA of green fluorescent protein (ds*GFP*) were used as control. Injection was carried out for 100 individual larvae in each group. Two days after injection, three larvae were randomly selected for total RNA extraction. The remaining larvae were allowed to develop into the pupal stage. Three of these from the group injected with ds*OfHEX1* that showed abnormal phenotypes and three from the control group were selected for transcriptional analysis of *OfHEX1* by real-time PCR as described above.

Protein Expression and Purification—Expression and purification of OfHex1 were carried out as described previously (24). Briefly, the gene encoding OfHex1 was amplified from the vector CTB557-2-1 (kept in our laboratory) by PCR using forward primer 5′-GCTTACGTAGAATTCGAGGACGTAGTATGGCGCTGGT-3′ and reverse primer 5′-TTAATTCGCGGCCGCTTAATGATGATGATGATGATGCGAGTAACAGTACCCCTC-3′. The expressed OfHex1 contained a His_6 tag at the C terminus. Single amino acid mutations were made by PCR using the following primer pairs: 5′-GCTTGTTCTCCTTACATCGGATGGCAG-3′ (forward) and 5′-GATGTAAGGAGAACAAGCGTTGTTACCAGC-3′ (reverse) for W490A; 5′-GGTGAGCCCCCATGCGGTCAGCTC-3′ (forward) and 5′-CGCATGGGGGCTCACCGCAGTATGATTTCC-3′ (reverse) for V327G; 5′-CCAAGTAGCTACCACCGGCGT-3′ (forward) and 5′-GTGGTAGCTACTTGGATAATG-3′ (reverse) for W448A; 5′-CCAAGTATTTACCACCGGCGT-3′ (forward) and 5′-GTGGTAAATACTTGGATAATG-3′ (reverse) for W448F; 5′-GCGCCCCCATGCGGTCAGCTCA-3′ (forward) and 5′-ACCGCATGGGGGCGCCACGCAG-3′ (reverse) for E328A; and 5′-CAGCCCCCATGCGGTCAGCTCA-3′ (forward) and 5′-ACCGCATGGGGGCTGCACGCAG-3′ (reverse) for E328Q. The PCR products were cloned into pPIC9 (Invitrogen) and transformed into *Pichia pastoris* GS115 by electroporation. Cells were cultured in BMMY broth (2% peptone, 1% yeast extract, 1% methanol, 1.34% yeast nitrogen base, and 0.1 M potassium phosphate (pH 6.0)) for 144 h, and methanol (1% of the total volume) was added every 24 h. Wild-type and mutant OfHex1 were purified from the culture supernatant by ammonium sulfate precipitation (65% saturation), affinity chromatography on an IMAC Sepharose High Performance column (GE Healthcare) followed by anion exchange chromatography on a Q Sepharose high performance column (GE Healthcare) (24).

Enzymology—Steady-state kinetics of wild-type and mutant OfHex1 were assayed using 4-methylumbelliferone-*N*-acetyl-β-D-glucosaminide (4MU-β-GlcNAc) (Sigma) as substrate. The reaction mixture (100 μl) contained 1–16 μM 4MU-β-GlcNAc and an appropriate amount of enzyme in Britton-Robinson's wide range buffer. After incubating at 25 °C for 5 min, 100 μl of 0.5 M glycine-NaOH (pH 10.3) was added to the sample to stop the reaction, and the fluorescence produced by the released 4-methylumbelliferone was quantified by a spectrofluorometer (Thermo Scientific Varioskan Flash, Thermo) using excitation and emission wavelengths of 360 and 405 nm, respectively.

Steady-state kinetics of wild type and of V327G and W490A mutants were also assayed using chitobiose ($(GlcNAc)_2$; Sigma) as substrate. The reaction mixture (50 μl) contained 33–100 μM $(GlcNAc)_2$ and 5 mM sodium phosphate buffer (pH 7.0). After incubating at 25 °C for 10 min, the hydrolytic products were analyzed by HPLC using TSKgel Amide-80 column (4.6 × 250 mm, Tosoh) on the Agilent 1200 HPLC system (Agilent) (2). The K_m and k_{cat} values of each enzyme were calculated by linear regression via Lineweaver-Burk plots.

The inhibition constants (K_i) were determined by steady-state kinetics using the same conditions, but the samples contained different concentrations of inhibitors. The K_i values were calculated by linear regression of data in Dixon plots.

Crystallization and Data Collection—Both native and inhibitor-bound OfHex1 were crystallized in the space group $P3_221$ within 2 weeks by vapor diffusion at 4 °C. The mother liquor of the native protein consisted of 100 mM HEPES (pH 7.0), 200 mM $MgCl_2$, and 30% PEG 400. The crystal of OfHex1 in complex with TMG-chitotriomycin was obtained by co-crystallization of the native protein with a 5-fold excess of TMG-chitotriomycin in the same mother liquor as that of native OfHex1, except at pH 7.5. Hanging drops were set up by mixing an aliquot of enzyme (7 mg/ml) with an equal amount of the mother liquor. Diffraction data were collected at the Shanghai Synchrotron Radiation Facility, BL-17U. All diffraction data were processed using the HKL2000 package (25).

Structure Determination and Refinement—The structures of free OfHex1 and OfHex1-TMG-chitotriomycin complex were solved by molecular replacement with MolRep (26) using the structure of human hexosaminidase B (Protein Data Bank code 1O7A) as the search model. Structure refinement was carried out by RefMac (27) and CNS (28). Model building was performed in Coot (29). The quality of the final model was checked by PROCHECK (30). The statistics of the data collection and structure refinement are summarized in Table 1. The coordinates of the native OfHex1 and of the OfHex1-TMG-chitotriomycin complex were deposited in the Protein Data Bank with accession numbers of 3NSM and 3NSN, respectively. All structural figures were prepared by PyMOL (DeLano Scientific LLC, San Carlos, CA).

TABLE 1
Data collection and structure refinement statistics for OfHex1

	OfHex1	OfHex1-TMG
Data collection		
Space group	$P3_221$	$P3_221$
Cell dimensions		
a, *b*, *c* (Å)	108.1, 108.1, 175.5	108.5, 108.5, 175.6
α, β, γ (degrees)	90.0, 90.0, 120.0	90.0, 90.0, 120.0
Resolution (Å)	49.63-2.10 (2.14-2.10)[a]	50.00-2.10 (2.14-2.10)
R_{sym} or R_{merge}	0.095 (0.299)	0.078 (0.342)
$I/\sigma I$	24.3 (2.3)	18.5 (2.6)
Completeness (%)	99.2 (99.9)	86.9 (74.9)
Redundancy	5.1 (4.5)	3.8 (3.2)
Refinement		
Resolution (Å)	2.10	2.10
No. of reflections	58,734	55,689
R_{work}/R_{free}	0.203/0.223	0.187/0.202
No. of atoms		
Protein	4615	4615
Ligand/ion	0	57
Water	429	444
Root mean square deviations		
Bond lengths (Å)	0.007	0.007
Bond angles (degrees)	1.095	1.190

[a] Values in parentheses are for highest resolution shell.

RESULTS

Temporal and Spatial Transcriptional Patterns of OfHEX1—The expression profile of *OfHEX1* was analyzed by real-time RT-PCR. Expression of *OfHEX1* was up-regulated before each molting stage during development of the late fourth instar larva (*4L*), late fifth instar larva (*5L5*), prepupa (*PP*), and late pupa (*P3*) (Fig. 1*A*). The expression level of OfHex1 reached its peak at the fifth instar day 5 and prepupa stages, which is about 10 times higher than that of fifth instar day 3 larva (*5L3* in Fig. 1). This demonstrated that transcription of *OfHEX1* was greatly up-regulated during pupation of *O. furnacalis*.

To determine whether transcription of *OfHEX1* is tissue-specific, larvae of two representative developmental stages (fifth instar days 3 and 5) were selected, and the levels of *OfHEX1* transcript in the integument and alimentary tracts were measured. Larvae at the fifth instar day 3 stage showed a considerable increase in body weight at a rate of 0.03 g/day, whereas those at the fifth instar day 5 stage had already stopped feeding and began to spin and prepare to pupate. As shown in Fig. 1*B*, the expression levels of *OfHEX1* in the integument and alimentary tract were similar at the fifth instar day 3 stage. However, at the fifth instar day 5 stage, the expression level of OfHEX1 in the integument was up-regulated more than 3-fold but remained unchanged in the alimentary tract. This demonstrated that the up-regulation of *OfHEX1* transcription was specific to the integument during the pupation of *O. furnacalis*.

RNAi of OfHEX1—Based on the data of temporal and spatial transcriptional patterns of *OfHEX1*, we proposed that this gene is involved in the pupation of *O. furnacalis.* To validate this proposal, gene-specific dsRNA was injected into fifth instar day 2 larvae of *O. furnacalis* to suppress the transcription of *OfHEX1*. Before pupation, most of the larvae injected with *OfHEX1* survived without any visible changes in phenotype and appeared similar to those injected with ds*GFP*. At the pupation stage, however, 20% of the ds*OfHEX1*-injected larvae showed abnormal phenotypes that were absent in ds*GFP*-injected larvae and died 1 or 2 days after pupation. The pupation process was obviously affected at different times (Fig.

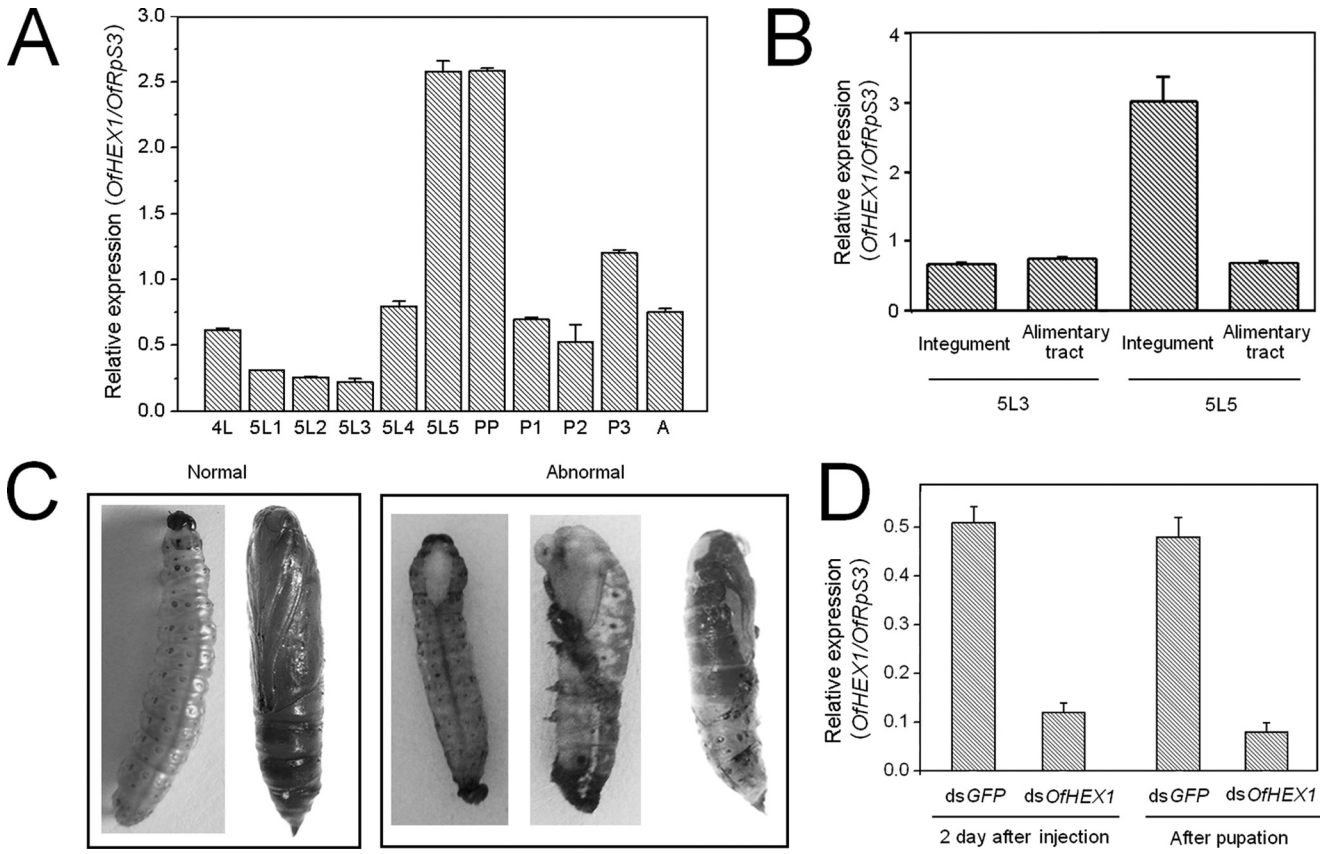

FIGURE 1. **Transcriptional pattern analysis and RNAi of *OfHEX1*.** *A*, transcriptional pattern of *OfHEX1* at different developmental stages of *O. furnacalis*. *4L*, fourth instar larvae; *5L1*, fifth instar larvae (1st day); *5L2*, fifth instar larvae (2nd day); *5L3*, fifth instar larvae (3rd day); *5L4*, fifth instar larvae (4th day); *5L5*, fifth instar larvae (5th day); *PP*, prepupae; *P1*, pupae (early); *P2*, pupae (medium); *P3*, pupae (late); *A*, adults. *B*, transcriptional pattern of *OfHEX1 in different tissues of O. furnacalis*. *C*, normal larva/pupa and three abnormal phenotypes of ds*OfHEX1*-injected insects. *D*, effect of RNAi on the transcriptional levels of *OfHEX1*. Data are the mean ± S.E. (*error bars*) from three independent experiments.

1*C*). Some abnormal phenotypes manifested only as a small opening at the back without further molting while the whole body still remained in the larval stage, but the white new cuticle was already visible at the opening (Fig. 1*C*, *first abnormal sample*). Some abnormal larvae shed half of their old cuticles, with the head capsules already moved to the middle of the body. The head and thorax became tanned, but the abdomen remained in the larval form (Fig. 1*C*, *second abnormal sample*). Other larvae with abnormal phenotypes shed most of the old cuticles and appeared as nascent pupae, but part of the old black cuticle with the head capsule still tightly adhered to the body and could not molt completely (Fig. 1*C*, *third abnormal sample*). Thus, it appeared that all of the *O. furnacalis* larvae with abnormal phenotypes failed to shed their old cuticles completely before new ones started to form underneath. Down-regulation of *OfHEX1* in ds*OfHEX1*-injected *O. furnacalis* was observed not only in the larvae after 2 days of injection but also in the larvae at the emergence of the abnormal phenotype (Fig. 1*D*). The result demonstrated that OfHex1 plays a vital role in the degradation of old cuticle during the pupation stage of *O. furnacalis*. *TcNAG1*, a homolog of *OfHEX1* from *T. castaneum*, has also been validated by RNAi to play a role in cuticular chitin turnover during insect metamorphosis (13). ds*TcNAG1*-injected insects failed to completely shed their old cuticles and finally died.

Overall Structure of an Insect β-N-Acetyl-D-hexosaminidase—OfHex1 was expressed as a secretory enzyme in *P. pastoris* and purified as described previously (24).

The crystal structure of the free OfHex1 reveals a homodimeric enzyme with the two monomers in the adjacent asymmetry units reconstructed by a crystallographic 2-fold symmetry axis adhering to each other in a side-by-side fashion. Each monomer is *N*-glycosylated at Asn^{164} and Asn^{375}. All of the 12 cysteine residues of each monomer contribute to the intradisulfide bonds (Cys^{31}–Cys^{59}, Cys^{36}–Cys^{55}, Cys^{316}–Cys^{373}, Cys^{326}–Cys^{331}, Cys^{478}–Cys^{491}, and Cys^{585}–Cys^{592}).

The interface between two monomers is formed mainly by loop regions of the $(\beta/\alpha)_8$-barrel with a buried area of ~2,853 $Å^2$/monomer, 2 times bigger than that of human dimeric HexB (1,612 $Å^2$) or HexA (1,587 $Å^2$) (Fig. 2*A*). Numerous hydrophobic bonds and five salt bridges at the dimer interface were revealed by PISA (available on the European Bioinformatics Institute Web site).

Each monomer of OfHex1 consists of a typical two-domain fold similar to those of the human (14–16) and bacterial (*S. plicatus* and *Paenibacillus* sp.) (17, 18, 22) enzymes. However, some significant differences can be seen, especially in the N and C termini as well as in the $(\beta/\alpha)_8$-barrel, where the active center is located.

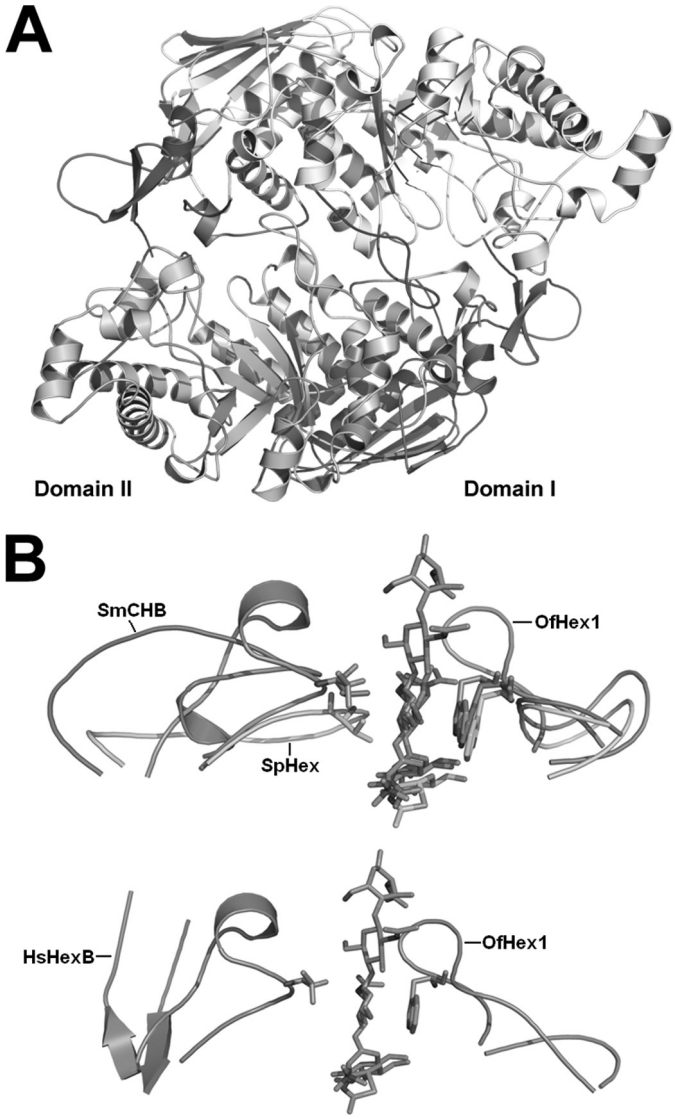

FIGURE 2. **Overall structure of OfHex1.** *A*, overall structures of dimeric OfHex1. Domain I and domain II are shown in *light blue* and *wheat*, respectively. Four unique structural elements in OfHex1 are shown in *different colors*. The N-terminal and C-terminal additional structures involved in dimerization are shown in *orange* and *red*, respectively. $L_{314-335}$ and $L_{478-496}$ are shown in *pink* and *green*, respectively. *B*, comparison of $L_{314-335}$ and $L_{478-496}$ in the OfHex1-TMG-chitotriomycin complex (*blue*) with corresponding regions in the SmCHB-chitobiose complex (1QBB) (*green*), SpHex-NGT complex (1HP5) (*pink*), and human HexB-NGT complex (1NP0) (*yellow*). The conserved residues Val^{327} (Val^{493} in SmCHB and Val^{276} in SpHex) and Trp^{490} (Trp^{685} of SmCHB and Trp^{408} of SpHex) are shown as *sticks*.

Domain I of OfHex1 consists of residues 23–205 following a 22-residue N-terminal signal peptide. Structural alignment indicated that domain I is conserved in most known β-*N*-acetyl-D-hexosaminidases (17–20, 22, 23). Besides the conserved six-stranded antiparallel β-sheets, there is one extra antiparallel β-strand and α-helix on the N terminus (residues 23–61, in *orange*) of OfHex1 (Fig. 2*A*). These extra segments appear to be important for dimerization through interaction with domain II of the adjacent monomer via residues 264–273, 306, 309, and 310.

Domain II of OfHex1 is formed by residues 208–594, which contains the active pocket within the classical $(\beta/\alpha)_8$-barrel segments. Like all known GH20 β-*N*-acetyl-D-hexosaminidases, OfHex1 also does not have helices α5 and α7. Unlike the other enzymes, OfHex1 contains an extended loop ($L_{361-366}$, residues 361–366) instead of the β4 strand. Because two catalytic residues, Asp^{367} and Glu^{368}, are located at the end of $L_{361-366}$, this change may bring the catalytic residues into closer proximity with the substrate. Two other loops, residues 314–335 ($L_{314-335}$ in *pink*) and residues 478–496 ($L_{478-496}$ in *green*), are rigid but appear functional (Fig. 2, *A* and *B*). $L_{314-335}$ is located between β3 and α3 and stabilized by two pairs of disulfide bonds, Cys^{326}–Cys^{331} and Cys^{316}–Cys^{373}. $L_{478-496}$ appears as a twisted "8" and is positioned parallel to its counterpart in the adjacent monomer by numerous interactions, suggesting its role in dimerization. Structural comparison showed that these two loops are present in bacterial GH20 β-*N*-acetyl-D-hexosaminidases, SpHex (17, 18) and SmCHB (19, 20), although much variation in amino acid composition exists in these two loops of the enzymes. Because SpHex and SmCHB belong to chitinolytic bacteria, one of these two loops may play a role in substrate specificity. The C terminus of OfHex1 consists of an additional α-helix followed by a loop-like structure (residues 575–594, in *red*) (Fig. 2*A*). These extra features may also be important for dimerization through interaction with domain II of the adjacent monomer.

Architecture of the Active Site—To gain insight into the active site of OfHex1, the crystal structure of the enzyme in complex with TMG-chitotriomycin was resolved to 2.1 Å (Fig. 3*B*). TMG-chitoriomycin is a linear pseudotetrasaccharide consisting of three sequentially arranged β-1,4-linked GlcNAcs and one *N*,*N*,*N*-triMe-D-$GlcNH_2$ at the non-reducing end (Fig. 3*A*) (32, 33). Compared with other known inhibitors that have one sugar moiety, it is the best mimic of natural substrates (chitooligosaccharides) for investigating the substrate-binding mode.

Overall, TMG-chitotriomycin binds OfHex1 at a deeper and larger pocket compared with those of human HexA and HexB (Fig. 3*C* and supplemental Fig. S1). Unlike dimeric HexA (16) or HexB (14, 15), the active pocket of each OfHex1 monomer is isolated and self-stabilized. The active pocket can be divided into two parts: the −1 subsite for catalysis and the +1 subsite for binding the +1 sugar unit of substrates.

It is clear that numerous intermolecular interactions are involved in locking TMG-chitotriomycin into the active site and positioning it for intramolecular nucleophilic attack (Fig. 3*C*). Like all known GH20 β-*N*-acetyl-D-hexosaminidases, the active site is highly conserved. Three tryptophan residues (Trp^{424}, Trp^{448}, and Trp^{524}) form a tight hydrophobic pocket (Fig. 3*C*). Together with Asp^{367} and Tyr^{475}, these tryptophan residues form the wall and the bottom of the active site. A conserved catalytic triad is formed by residues Asp^{249}, His^{303}, and Glu^{368} and stabilized by hydrogen bonds among these residues. The catalytic H_2O(II) (Fig. 3*C*), localized at the end of the catalytic triad, is stabilized by Glu^{368} through a hydrogen bond. Another water molecule, H_2O(I), functions to stabilize Glu^{328} and Glu^{368} (Fig. 3*C*).

B-factors of each sugar unit of TMG-chitotriomycin were obtained: 20.94 (*N*,*N*,*N*-triMe-D-$GlcNH_2$), 23.72 (GlcNAcI), 41.18 (GlcNAcII), and 69.37 (GlcNAcIII). *N*,*N*,*N*-triMe-D-

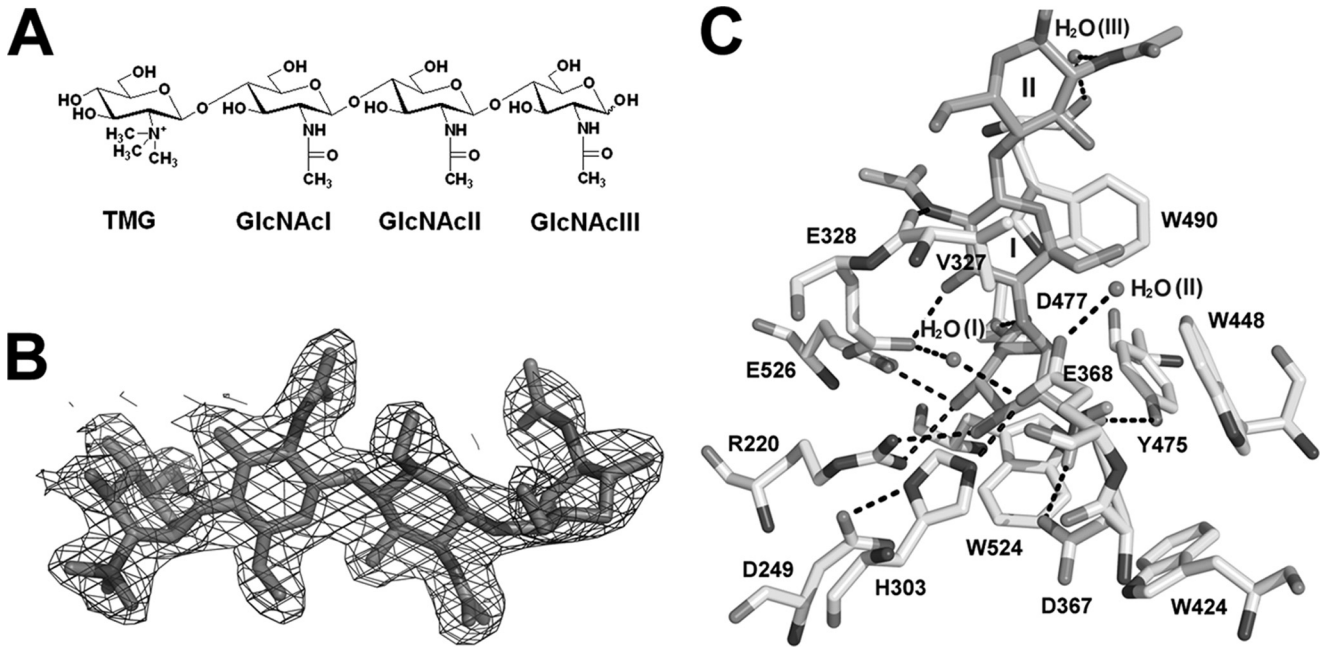

FIGURE 3. **The active site of OfHex1.** *A*, structure of TMG-chitotriomycin. *B*, electron density of TMG-chitotriomycin. The $F_o - F_c$ map is contoured at the 3σ level. *C*, intermolecular interactions between TMG-chitotriomycin and OfHex1. Hydrogen bonds are shown in *black dashes*.

$GlcNH_2$ binds tightly to the active pocket at the −1 subsite in $^{1,4}B$ conformation by stacking force provided by the indolyl group of Trp^{524}. Like $(GlcNAc)_2$ in the complex of SmCHB (19), the plane of the −1 sugar is rotated around the glycosidic linkage by about 90°. The positively charged *N,N,N*-triMe group interacts with negatively charged catalytic Asp^{367} and Glu^{368} and forms hydrogen bonds with Asp^{367}, Glu^{368}, and Tyr^{475}.

In addition, other hydrogen bonds are formed between the sugar unit and active sites residues, including those between O-1 and Glu^{368}, O-3 and Arg^{220}, and O-4 and both Arg^{220} and Glu^{526} as well as between O-6 and both Asp^{477} and Trp^{490} (Fig. 3*C*). As revealed by structural alignment, the binding mode of *N,N,N*-triMe-D-$GlcNH_2$ is very similar to that of other known ligands of GH20 β-*N*-acetyl-D-hexosaminidases (supplemental Fig. S2). This is also in good agreement with amino acid sequence alignment (Fig. 4). The above observations indicate that TMG-chitotriomycin mimics the natural substrate to block the approach of the substrate to the enzyme's active site.

The GlcNAcI component adjacent to *N,N,N*-triMe-D-$GlcNH_2$ is localized at the +1 subsite in the active pocket. It is sandwiched by the isopropyl group of Val^{327} and the indolyl group of Trp^{490} (Fig. 3*C*). The indolyl group of Trp^{490} is stacked against the sugar ring in $^1C_4$ conformation, with a short hydrogen bond (2.48 Å) formed between O-3 and Glu^{328} and between the nitrogen of the acetamido group and Val^{327}. Both GlcNAcII and GlcNAcIII are pointed away from the active pocket and are exposed to solvent. The GlcNAcII component in $^1C_4$ conformation is stabilized by two pairs of hydrogen bonds, one with Val^{327} and the other with Trp^{490} via a water molecule, thus blocking the entrance of the active pocket. The GlcNAcIII component in $^0S_2$ conformation remains pendulous.

The kinetics of V327G and W490A mutants, determined using 4MU-β-GlcNAc and $(GlcNAc)_2$ as substrates, are shown in Table 2. 4MU-β-GlcNAc contains the −1 sugar, whereas $(GlcNAc)_2$ contains both −1 and +1 sugars; therefore, 4MU-β-GlcNAc was used for investigating the catalytic activity of OfHex1 and $(GlcNAc)_2$ for sugar binding preference. The replacement of Val^{327} with glycine resulted in slight decrease in K_m and a 20–60% loss in catalytic activity as seen with a drop in k_{cat} (Table 2), indicating that mutation at Val^{327} affected both substrate binding and catalysis while having no effect on the enzyme's preference toward +1 or −1 sugar binding. In contrast, replacement of Trp^{490} with alanine led to a 13-fold increase in K_m with $(GlcNAc)_2$ as a substrate and a 62% loss in catalytic activity when 4MU-β-GlcNAc was used as substrate, suggesting that Trp^{490} is essential for binding the +1 sugar (Table 2). Further evidence supporting the important role of Trp^{490} in binding the +1 sugar came from an inhibition study whereby the K_i of W490A for TMG-chitotriomycin decreased by 2,277-fold relative to that of wild type, whereas the K_i of V327G showed no change in K_i (Table 3).

Inhibitor Binding Induced Significant Conformational Changes in the Active Site—Family 20 glycosyl hydrolases catalyze the breakdown of β-glycosidic bonds of various glycoconjugates from the non-reducing end by a mechanism known as the substrate assistant-retaining mechanism, which was first elucidated for bacterial and human β-N-acetyl-D-hexosaminidases (17–20). In this mechanism, the catalytic glutamate first acts as an acid that attacks the glycosidic oxygen and then as a base that abstracts a proton from a water molecule. The catalytic asparate is required to stabilize the positively charged nitrogen of the 2-acetamido group, which is involved in the formation of a transient oxazolinium intermediate (17–20). As revealed by the crystal structure of OfHex1, the two catalytic residues (Glu^{368} and Asp^{367}) the catalytic H_2O (H_2O(II)), and the catalytic triad (Asp^{249}–His^{303}–Glu^{368}) are highly conserved.

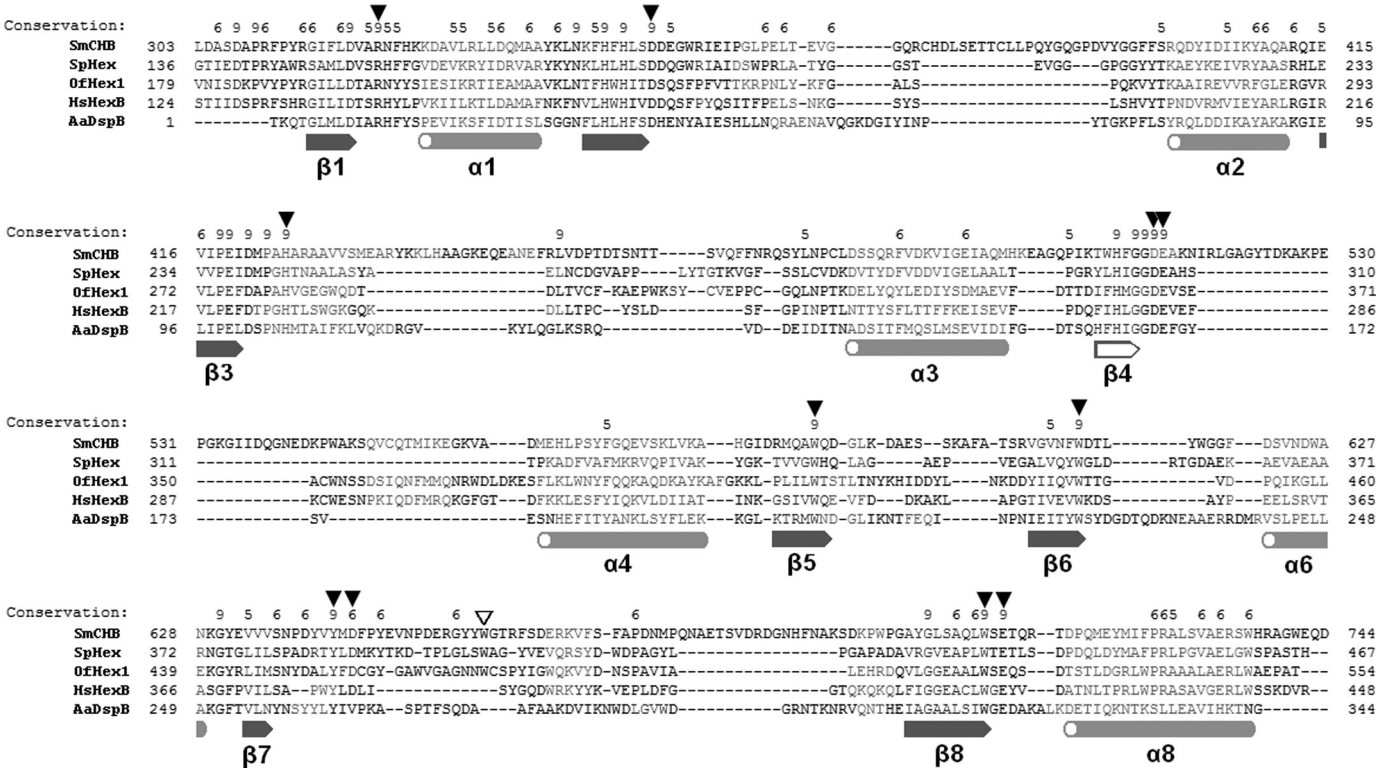

FIGURE 4. **Sequence alignment of catalytic domains of GH20 β-*N*-acetyl-D-hexosaminidases.** Structure-based alignment was performed with PROMALS3D (31). α-Helices and β-sheets are shown in *orange* and *blue*, respectively (common ones are *filled*, and uncommon ones are *unfilled*). Important residues are indicated by *triangles* (common ones are *filled*, and uncommon ones are *unfilled*).

TABLE 2

Kinetic parameters of WT and mutants of OfHex1

Data are the means ± S.D. of three determinations.

	Substrate	K_m	k_{cat}	k_{cat}/K_m
		mM	s^{-1}	$s^{-1}\ mM^{-1}$
WT	4MU-β-GlcNAc	0.107 ± 0.009	434.7 ± 13.3	4063
V327G	4MU-β-GlcNAc	0.070 ± 0.003	189 ± 4.9	2700
W490A	4MU-β-GlcNAc	0.100 ± 0.006	167.6 ± 4.1	1676
WT	$(GlcNAc)_2$	0.148 ± 0.009	507.4 ± 32.5	3428
V327G	$(GlcNAc)_2$	0.126 ± 0.008	337 ± 27	2675
W490A	$(GlcNAc)_2$	1.875 ± 0.042	449.6 ± 19.8	239.8
W448A	4MU-β-GlcNAc	0.223 ± 0.011	0.469 ± 0.032	2.103
W448F	4MU-β-GlcNAc	0.149 ± 0.008	0.567 ± 0.044	3.805
H433A	4MU-β-GlcNAc	0.095 ± 0.004	0.313 ± 0.018	3.295
E328A	4MU-β-GlcNAc	0.096 ± 0.004	356 ± 17.3	3708
E328Q	4MU-β-GlcNAc	0.105 ± 0.005	349 ± 15.4	3324

TABLE 3

TMG-chitotriomycin inhibition against WT and mutants of OfHex1

Data are the means ± S.D. of three determinations.

Enzyme	K_i	K_i of mutant OfHex1/K_i of WT OfHex1
	μM	
WT	0.065	1
V327G	0.077	1.18
W490A	148	2277

It is worthy of note that binding of TMG-chitotriomycin has induced significant conformational changes in OfHex1 compared with inhibitor-free enzyme (Fig. 5*A*). Because such an inhibitor-triggered conformational change has not been observed for any of the known GH20 β-*N*-acetyl-D-hexosaminidases, including the human enzymes HexA and HexB and the bacterial enzymes SpHex and SmCHB, (14–20), OfHex1 is therefore very different from other β-*N*-acetyl-D-hexosaminidases in this regard.

At the −1 subsite of the active pocket, Glu^{368} and Asp^{367} are rotated about 180 and 90°, respectively, after binding TMG-chitotriomycin. Two other residues, His^{303} and Trp^{448}, are rotated about 30 and 45°, respectively (Fig. 5*A*). These movements have resulted in the establishment of two new hydrogen bonds, both of which are linked to Glu^{368}: one connecting Glu^{368} with His^{303} via Asp^{249} and the other connecting Glu^{368} with Glu^{328} via the catalytic H_2O (Fig. 5*A*). Mutation of Glu^{328} to alanine or glutamine resulted in a 19% decrease in catalytic activity in terms of k_{cat} value (Table 2). We assume that the hydrogen bond networks function to stabilize Glu^{368}.

It is very interesting to note that the movements of Glu^{368} together with Trp^{448} would lead either to an open- or close-active pocket, and the side chain of Trp^{448} would act as a lid for this pocket (Fig. 5*B*). After binding with TMG-chitotriomycin, the side chains of Glu^{368} and Trp^{448} are rotated to face the active site to form a closed hydrophobic pocket. In the absence of the inhibitor, the active site remains open and is accessible to solvent. The unique open-close mechanism of the active site would enable OfHex1 not only to carry out catalysis but also to facilitate substrate binding or release of product. Although no such conformational change has been found in other known GH20 enzymes (14–23), conformational change has been observed in GH84 β-*N*-acetyl-D-glucosaminidase (CpGH84) after binding with inhibitor due to a 180° rotation by the catalytic aspartate (Asp^{298}) (34, 35). Before the binding of substrate, the side chain of the catalytic Glu^{368} of OfHex1 is connected to Thr^{427} via two hydrogen bonds, whereas Asp^{298} of CpGH84 is stabilized by an intramolecular hydrogen bond (34, 35).

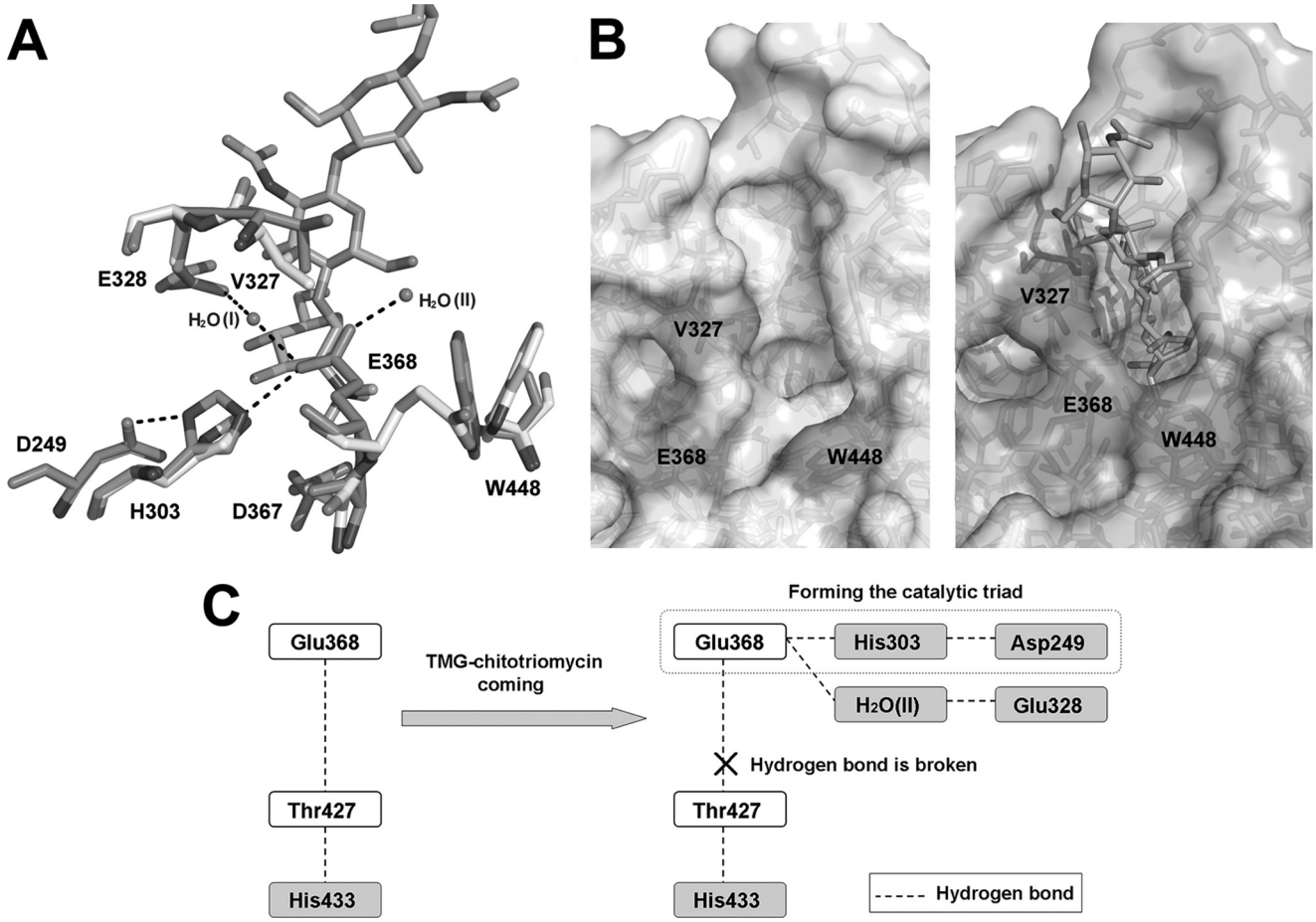

FIGURE 5. **Conformational changes induced by inhibitor binding at the active site.** *A*, conformational changes of +1 subsite residues (Val^{327} and Glu^{328}) and −1 subsite residues (His^{303}, Asp^{367}, Glu^{368}, and Trp^{448}) and two hydrogen bond networks (Asp^{249}–His^{303}–Glu^{368} and Glu^{328}–H_2O(I)–Glu^{368}) are shown. The spatial arrangements of these residues before and after TMG-chitotriomycin binding are shown in *white* and *blue*, respectively. The hydrogen bond networks are shown in *black dashes*. *B*, open and closed states of the active pocket. *C*, model explaining the changes in the coupling effects of the hydrogen-bonding network induced by inhibitor binding at the active site.

The replacement of Trp^{448} by alanine resulted in a 2-fold increase in K_m but a 927-fold decrease in k_{cat} and a 1900-fold decrease in k_{cat}/K_m (Table 2), meaning that the hydrophobic and large stereo indolyl group of Trp^{448} is essentially important for the "open-close" mechanism. Furthermore, when Trp^{448} was replaced by phenylalanine, which contains a plane-aromatic ring, little change in K_m occurred, but k_{cat} decreased more than 1,000-fold, resulting in an overall decrease in k_{cat}/K_m, indicating that the phenyl group cannot substitute for the indolyl group (Table 2). Trp^{448} is stabilized by a hydrogen bond with $L_{425-433}$ (residues 425–433) through its indolyl nitrogen. Trp^{448} is highly conserved in other species (*e.g.* Trp^{405} in human HexB, Trp^{344} in SpHex, and Trp^{616} in SmCHB (Fig. 4)) (14–20). Unlike OfHex1, the tryptophan residues of these enzymes interact with α-helices residues, showing less flexibility as far as the indolyl group is concerned. This unique flexibility conferred by Trp^{448} in OfHex1 is reflected in the active pocket lid.

At the +1 subsite, the GlcNAcI component of TMG-chitotriomycin is sandwiched and stabilized by Val^{327} and Trp^{490}. Compared with free OfHex1, the Val^{327} in the inhibitor-bound enzyme is rotated about 90° and moved slightly, and this has the effect of increasing the distance between Val^{327} and Trp^{490} from about 7 Å to 8.5 Å (Fig. 5*A*). Thus, the side chain of Val^{327} is hydrogen-bonded to GlcNAcII and GlcNAcIII of TMG-chitotriomycin (Fig. 3*C*), and the isopropyl group of Val^{327} is positioned parallel to the indolyl group of Trp^{490}. In this state, the +1 sugar in TMG-chitotriomycin can be sandwiched firmly. Although OfHex1 and bacterial chitinolytic β-*N*-acetyl-D-hexosaminidases (SmCHB and SpHex) share a conserved +1 subsite architecture that is characterized by Val^{327} (Val^{493} in SmCHB and Val^{276} in SpHex) and Trp^{490} (Trp^{685} in SmCHB and Trp^{408} in SpHex) (17–20) (Fig. 2*B*), it is the only β-*N*-acetyl-D-hexosaminidase to show obvious conformational changes after ligand binding.

DISCUSSION

Insects contain several β-*N*-acetyl-D-hexosaminidases that have different physiological roles. However, until now, what determines the specialized physiological roles of these enzymes remains unknown.

We have shown here via RNAi that OfHex1 plays a key role during the pupation of *O. furnacalis*. OfHex1 shares 31–33% similarity in amino acid sequences with human lysosomal β-*N*-acetyl-D-hexosaminidases (human HexB as a representative) and 21–26% with bacterial chitinolytic β-*N*-acetyl-D-

hexosaminidases (SmCHB as a representative), and the structural comparison presented here has given some insights into how the insect chitinolytic β-*N*-acetyl-D-hexosaminidases may carry out the degradation of chitin.

Insect OfHex1 Versus Human HexA and HexB—Human β-*N*-acetyl-D-hexosaminidases are known to be lysosomal enzymes having optimal pH at 3–4, whereas OfHex1 is an extracellular enzyme with optimal pH at 7. The physiological substrates for mammal lysosomal β-*N*-acetyl-D-hexosaminidases and their plant counterparts are mainly branching sugar chains on glycolipids and glycoproteins (3, 9, 10). In contrast, the physiological substrates of chitinolytic β-*N*-acetyl-D-hexosaminidases are linear chitooligosaccharides. The differences in substrate specificity between the chitinolytic and human β-*N*-acetyl-D-hexosaminidases can be explained by the differences in the structures of their active sites.

Chitinolytic β-*N*-acetyl-D-hexosaminidases, such as OfHex1 and SmCHB, have a deeper substrate binding pocket that includes both −1 and +1 subsites, whereas lysosomal β-*N*-acetyl-D-hexosaminidases, such as the human enzymes, have only the −1 subsite (14–16). The two conserved residues, Trp^{490} and Val^{327}, at the +1 subsite of OfHex1 are responsible for binding the +1 sugar by hydrogen bonds and π-π stacking interactions as well as forming the walls of the +1 sugar-binding cleft in OfHex1. These two residues are structurally conserved in the bacterial enzymes (Trp^{685} and Val^{493} in SmCHB and Trp^{408} and Val^{276} in SpHex) (Fig. 2*B*) but are not present in human HexA and HexB (14, 15) (Fig. 2*B*). Thus, compared with OfHex1 as well as SmCHB and SpHex, the binding pockets of the human enzymes are exposed to physiological substrates (*e.g.* glycolipid G_{A2}), but only the −1 sugar can be accommodated. The rest of the molecule cannot be positioned in the binding pocket and instead remains exposed to solvent (14–16).

Furthermore, OfHex1 contains two conserved loops, $L_{314-335}$ and $L_{478-496}$, which are absent in human β-*N*-acetyl-D-hexosaminidases (Fig. 2*B*). It is worth noting that Val^{327} and Trp^{490} of OfHex1 are located within these two loops. Because these loops are localized at the entrance of the active pocket, they may serve as a scaffold for Val^{327} and Trp^{490} to stabilize the +1 sugar of the substrate. We think that all chitinolytic β-*N*-acetyl-D-hexosaminidases probably have a +1 subsite, which comprises the conserved tyrptophan and valine, to stabilize the +1 sugar of the substrate. SmCHB and SpHex also contain these loops, although the amino acid sequences that constitute these loops are quite different except for the conserved valine and tryptophan (17–20). Thus, we believe these loop structures enable chitinolytic β-*N*-acetyl-D-hexosaminidases to bind long chained and linear chained substrates like chitooligosaccharides, whereas HexA/B with a shallow active pocket is capable of binding branching *N*-glycans (*e.g.* (GlcNAcβ1,2Manα1,b)(GlcNAcβ1,2Manα1,3)-Manβ1,4GlcNAcβ1,4GlcNAc-PA) or branching substrates with bulky substituents, such as G_{M2} and G_{A2} gangliosides. OfHex1 cannot use GnGn-PA as a substrate (2).

OfHex1 Versus Bacterial SmCHB—Like OfHex1, SmCHB is a chitinolytic β-*N*-acetyl-D-hexosaminidase that could degrade chitooligosaccharides and shares the conserved structural elements for binding the +1 sugar of the substrate. However, there are some differences between them. First, their overall structures are very different. OfHex1 is a homodimeric protein with two identical catalytic monomers, whereas SmCHB is a monomeric protein consisting of four domains, including one catalytic domain (19, 20). Therefore, although the two loops ($L_{314-335}$ and $L_{478-496}$ in OfHex1) at the +1 subsite can be found in the SmCHB (Fig. 2*B*), the loop length and amino acid composition as well as the roles in stabilizing the dimeric form are different.

OfHex1 is also distinguished from SmCHB by the big conformational changes between the free and inhibitor-bound enzymes. The structures of SmCHB as well as other known β-*N*-acetyl-D-hexosaminidases remain the same as their free forms after binding with inhibitors except for some minor conformational changes at the active pockets (19, 20). The conformational changes of OfHex1 initiated by binding with inhibitor has given rise to a unique mechanism that we called the "open-close" mechanism (Fig. 5*C*). In the "open" state (free enzyme), the side chain of Glu^{368} interacts with Thr^{427} via its side chain and nitrogen atom through hydrogen bonds of 2.71 and 2.94 Å, respectively. Thr^{427} is further stabilized by His^{433} through a hydrogen bond of 2.58 Å. In the "close" state (inhibitor-bound), the side chain of Glu^{368} is rotated 180° to form hydrogen bonds with His^{303}, which is also rotated by about 30°. Together with Asp^{249}, a catalytic triad is formed, and this has the effect of extending the hydrogen bond between Thr^{427} and His^{433} to 2.69 Å. The loss of activity (~1389-fold) revealed by H433A mutant suggests that His^{433} is very important with respect to stabilizing the hydrogen bond network necessary for catalytic efficiency.

Selective Inhibition Mechanism of TMG-chitotriomycin—TMG-chitotriomycin, which occurs naturally in Actinomycetes *Streptomyces anulatus* (32), has recently been synthesized by Yu *et al.* (33). It is the first reported inhibitor that shows specific inhibition against β-*N*-acetyl-D-hexosaminidases from chitin-containing organisms (32). The mechanism of selective inhibition has not yet been proven.

So far, based on the observations of intermolecular interactions between OfHex1 and TMG-chitotriomycin (Fig. 3*C*), the *N*,*N*,*N*-triMe-D-$GlcNH_2$ component appears to contribute most of the inhibitory activity of TMG-chitotriomycin, which functions as a substrate analog for β-*N*-acetyl-D-hexosaminidases. Therefore, one may deduce that *N*,*N*,*N*-triMe-D-$GlcNH_2$ alone would be a strong inhibitor or at least exhibits inhibitory activity. Usuki *et al.* (32) reported that *N*,*N*,*N*-triMe-D-$GlcNH_2$ is inactive against the insect GlcNAcase from *Spodoptera litura*. Similarly, we did not observe any inhibition exerted by *N*,*N*,*N*-triMe-D-$GlcNH_2$ against OfHex1 or against bacterial, plant, and mammalian β-*N*-acetyl-D-hexosaminidases, suggesting that other components of TMG-chitotriomycin are required for inhibition. Based on the crystal structure of OfHex1 complexed with TMG-chitotriomycin, two parts of this inhibitor are presumed to be responsible for the selective inhibition of OfHex1. First, the +1 subsite, which comprises Val^{327}, Trp^{490}, and Glu^{328}, can interact with the GlcNAcI component of TMG-chitotriomycin by both hydrophobic stacking and hydrogen bonding (Fig. 3*C*). These forces would stabilize GlcNAcI, which in turn sta-

bilizes the *N,N,N*-triMe-D-GlcNH$_2$ component that directly binds to the −1 subsite in the active pocket. It is interesting to note that Val^{327} and Trp^{490} are conserved in the bacterial SpHex (Val^{276} and Trp^{408}) and SmCHB (Val^{493} and Trp^{685}), both of which are capable of degrading chitooligosaccharides (Fig. 2*B*). Second, these chitinolytic β-*N*-acetyl-D-hexosaminidases, including OfHex1 and bacterial SpHex and SmCHB, have a deeper active pocket that can tightly bind both the −1 and +1 sugar units of GlcNAc, whereas human HexA and HexB have a shallower active pocket that merely binds the −1 sugar unit (supplemental Fig. S1). Without the presence of GlcNAcI at the +1 subsite, *N,N,N*-triMe-D-GlcNH$_2$, which is twisted through a 90° angle, could not be stabilized within a larger active pocket. W490A showed a K_m similar to that of wild-type when using a substrate with one sugar (4MU-β-GlcNAc), suggesting that the replacement of tryptophan with alanine would not affect substrate binding affinity at the −1 subsite (Table 2). However, the K_i of TMG-chitotriomycin dramatically increased more than 2,000-fold, suggesting that Trp^{490} is very important for binding long chitooligosaccharides (Table 3). These results have confirmed that the −1 and +1 sugars of the inhibitor together with Trp^{490} are essential for substrate binding. Because human HexA and HexB do not have the +1 subsite, it is not surprising that TMG-chitotriomycin is not an inhibitor for the human lysosomal β-*N*-acetyl-D-hexosaminidases. Thus, the mechanism of selective inhibition of TMG-chitotriomycin against OfHex1 is now elucidated.

In summary, OfHex1 is an insect chitinolytic β-*N*-acetyl-D-hexosaminidase that has been shown to play a vital role during the pupation of *O. furnacalis*. The structural alignment of OfHex1 with other enzymes revealed that OfHex1 is functionally specialized, and such a property is conferred by an open-close mechanism, as well as the unique architecture of the substrate binding site of the enzyme. Two residues, Trp^{448} and Trp^{490}, have been proven to be highly essential for catalysis and inhibition by TMG-chitotriomycin, as seen with a loss of more than 2,000-fold activity when these two residues were mutated. This work is the first to identify an important insect β-*N*-acetyl-D-hexosaminidase by functional and structural methods and may provide important clues for the design of species-specific pesticides.

Acknowledgments—We thank all of the staff at beamline BL17U of the Shanghai Synchrotron Radiation Facility (China). We thank Professor Biao Yu (Institute of Organic Chemistry, Chinese Academy of Science) for kindly providing the TMG-chitotriomycin and Professor Kang-Lai He (Institute of Plant Protection, Chinese Academy of Agricultural Science) for generously providing the insect, Asian corn borer. We thank Dr. Alan K. Chang (Dalian University of Technology) for revising the language of the manuscript.

REFERENCES

1. Intra, J., Pavesi, G., and Horner, D. S. (2008) *BMC Evol. Biol.* **8,** 214
2. Yang, Q., Liu, T., Liu, F., Qu, M., and Qian, X. (2008) *FEBS J.* **275,** 5690–5702
3. Mahuran, D. J. (1999) *Biochim. Biophys. Acta* **1455,** 105–138
4. Okada, T., Ishiyama, S., Sezutsu, H., Usami, A., Tamura, T., Mita, K., Fujiyama, K., and Seki, T. (2007) *Biosci. Biotechnol. Biochem.* **71,** 1626–1635
5. Aumiller, J. J., Hollister, J. R., and Jarvis, D. L. (2006) *Protein Expr. Purif.* **47,** 571–590
6. Miranda, P. V., González-Echeverría, F., Blaquier, J. A., Mahuran, D. J., and Tezón, J. G. (2000) *Mol. Hum. Reprod.* **6,** 699–706
7. Cattaneo, F., Ogiso, M., Hoshi, M., Perotti, M. E., and Pasini, M. E. (2002) *Insect. Biochem. Mol. Biol.* **32,** 929–941
8. Cattaneo, F., Pasini, M. E., Intra, J., Matsumoto, M., Briani, F., Hoshi, M., and Perotti, M. E. (2006) *Glycobiology* **16,** 786–800
9. Strasser, R., Bondili, J. S., Schoberer, J., Svoboda, B., Liebminger, E., Glössl, J., Altmann, F., Steinkellner, H., and Mach, L. (2007) *Plant Physiol.* **145,** 5–16
10. Gutternigg, M., Kretschmer-Lubich, D., Paschinger, K., Rendić, D., Hader, J., Geier, P., Ranftl, R., Jantsch, V., Lochnit, G., and Wilson, I. B. (2007) *J. Biol. Chem.* **282,** 27825–27840
11. Léonard, R., Rendic, D., Rabouille, C., Wilson, I. B., Préat, T., and Altmann, F. (2006) *J. Biol. Chem.* **281,** 4867–4875
12. Geisler, C., Aumiller, J. J., and Jarvis, D. L. (2008) *J. Biol. Chem.* **283,** 11330–11339
13. Hogenkamp, D. G., Arakane, Y., Kramer, K. J., Muthukrishnan, S., and Beeman, R. W. (2008) *Insect. Biochem. Mol. Biol.* **38,** 478–489
14. Mark, B. L., Mahuran, D. J., Cherney, M. M., Zhao, D., Knapp, S., and James, M. N. (2003) *J. Mol. Biol.* **327,** 1093–1109
15. Maier, T., Strater, N., Schuette, C. G., Klingenstein, R., Sandhoff, K., and Saenger, W. (2003) *J. Mol. Biol.* **328,** 669–681
16. Lemieux, M. J., Mark, B. L., Cherney, M. M., Withers, S. G., Mahuran, D. J., and James, M. N. (2006) *J. Mol. Biol.* **359,** 913–929
17. Mark, B. L., Vocadlo, D. J., Knapp, S., Triggs-Raine, B. L., Withers, S. G., and James, M. N. (2001) *J. Biol. Chem.* **276,** 10330–10337
18. Williams, S. J., Mark, B. L., Vocadlo, D. J., James, M. N., and Withers, S. G. (2002) *J. Biol. Chem.* **277,** 40055–40065
19. Tews, I., Perrakis, A., Oppenheim, A., Dauter, Z., Wilson, K. S., and Vorgias, C. E. (1996) *Nat. Struct. Biol.* **3,** 638–648
20. Prag, G., Papanikolau, Y., Tavlas, G., Vorgias, C. E., Petratos, K., and Oppenheim, A. B. (2000) *J. Mol. Biol.* **300,** 611–617
21. Ramasubbu, N., Thomas, L. M., Ragunath, C., and Kaplan, J. B. (2005) *J. Mol. Biol.* **349,** 475–486
22. Sumida, T., Ishii, R., Yanagisawa, T., Yokoyama, S., and Ito, M. (2009) *J. Mol. Biol.* **392,** 87–99
23. Langley, D. B., Harty, D. W., Jacques, N. A., Hunter, N., Guss, J. M., and Collyer, C. A. (2008) *J. Mol. Biol.* **377,** 104–116
24. Liu, T., Liu, F., Yang, Q., and Yang, J. (2009) *Protein Expr. Purif.* **68,** 99–103
25. Otwinowski, Z., and Minor, W. (1997) *Methods Enzymol.* **276,** 307–326
26. Vagin, A., and Teplyakov, A. (1997) *J. Appl. Cryst.* **30,** 1022–1025
27. Murshudov, G. N., Vagin, A. A., and Dodson, E. J. (1997) *Acta Crystallogr. D Biol. Crystallogr.* **53,** 240–255
28. Brünger, A. T., Adams, P. D., Clore, G. M., DeLano, W. L., Gros, P., Grosse-Kunstleve, R. W., Jiang, J. S., Kuszewski, J., Nilges, M., Pannu, N. S., Read, R. J., Rice, L. M., Simonson, T., and Warren, G. L. (1998) *Acta Crystallogr. D Biol. Crystallogr.* **54,** 905–921
29. Emsley, P., and Cowtan, K. (2004) *Acta Crystallogr. D Biol. Crystallogr.* **60,** 2126–2132
30. Laskowski, R. A., Macarthur, M. W., Moss, D. S., and Thornton, J. M. (1993) *J. Appl. Crystallogr.* **26,** 283–291
31. Pei, J., Kim, B. H., and Grishin, N. V. (2008) *Nucleic Acids Res.* **36,** 2295–2300
32. Usuki, H., Nitoda, T., Ichikawa, M., Yamaji, N., Iwashita, T., Komura, H., and Kanzaki, H. (2008) *J. Am. Chem. Soc.* **130,** 4146–4152
33. Yang, Y., Li, Y., and Yu, B. (2009) *J. Am. Chem. Soc.* **131,** 12076–12077
34. Rao, F. V., Dorfmueller, H. C., Villa, F., Allwood, M., Eggleston, I. M., and van Aalten, D. M. (2006) *EMBO J.* **25,** 1569–1578
35. He, Y., Martinez-Fleites, C., Bubb, A., Gloster, T. M., and Davies, G. J. (2009) *Carbohydr. Res.* **344,** 627–631